

Full Set of Superconducting Parameters of K_3C_{60}

Ren-Shu Wang,^{1,2} Di Peng,² Li-Na Zong,² Zeng-Wei Zhu,³ and Xiao-Jia Chen^{2,1,*}

¹*School of Science, Harbin Institute of Technology, Shenzhen 518055, China*

²*Center for High Pressure Science and Technology Advanced Research, Shanghai 201203, China*

³*Wuhan National High Magnetic Field Center, Wuhan 430074, China*

(Dated: August 9, 2022)

The superconducting parameters are the key for building or identifying the theory responsible for the mechanism of superconductivity. Such parameters for fulleride superconductors have not been well established despite the tremendous efforts over the past 30 years. Here we provide a full set of parameters through a systematic study on a well-characterized K_3C_{60} sample. The obtained high upper critical field of 33.0 ± 0.5 T from the direct electrical transport measurements together with the relatively high critical temperature and large critical current density classifies K_3C_{60} as a promising three-dimensional superconducting magnet material with the advantage of the rich carbon abundance on the Earth. This high upper critical field along with the large reduced superconducting energy gap and strong phonon self-energy effect supports the strong electron-phonon coupling interactions in this superconductor. The evaluation of all self-consistently obtained parameters suggests the unconventional nature of the superconductivity for K_3C_{60} with the joint contributions from the strong electron-phonon coupling and electron correlations. These results and findings are important not only for fundamentally understanding the superconductivity in fullerenes but also for future superconducting magnet developments and applications.

I. INTRODUCTION

The discovery of superconductivity in alkali fullerenes with the critical temperature T_c going from 18-19 K for K_3C_{60} [1] through 28-29 K for Rb_3C_{60} [2] to 38-40 K for Cs_3C_{60} [3–5] is an important event in modern science after the birth of the new form of carbon called ‘buckminsterfullerene’ or in short fullerene [6]. Apparently, these three-dimensional molecular solids are different in structure from the early discovered high- T_c cuprates and recently discovered twisted graphene [7]. They in reality share the similar superconducting phase diagram emerging from neighbouring Mott insulating state [4, 5, 7]. This similarity fuels the hope to solve the long-standing puzzle of the mechanism of superconductivity in cuprates once knowing the key factors that govern superconductivity in fullerenes due to the relatively easy realization of superconductivity with high T_c in fullerenes compared to the need of precise tuning in graphene, another purely C-based superconductor.

The crucial examination of the theory highly depends on the superconducting parameters. Take the first fullerene superconductor K_3C_{60} as an example, the large differences of these parameters from the experiments make the comparisons with the theory difficult [8, 9]. Conducting electrical transport measurements to realize the zero resistance state, known as one of the two essential features of a superconductor, has long been a challenge in the characterization of its superconductivity. Therefore, the characterization of fullerene superconductors has mainly been performed based on magnetization measurements [1, 10–12] due to the challenges in handling

the air-sensitive samples [13, 14]. Among the several electrical transport studies on K_3C_{60} [15–17], magnetic characterizations were absent. In fact, the first experimental evidence for supporting superconductivity in K_3C_{60} from the zero-resistance state and Meissner effect was obtained from different samples [1]. The airtight devices were developed to measure the resistivity for films [1, 17–19] and single crystals [20, 21] with the observed zero-resistance state in the superconducting state. Meanwhile, some residual resistances often appeared at low temperatures in the electrical transport measurements on single crystals [15, 22, 23], probably due to the limited crystallinity in films [1, 17, 18] or uncontrolled alkali distribution in single crystals [15, 22, 23]. Alternatively, the resistivity was inferred from some contactless methods [16, 24]. However, these techniques brought about large residual surface resistance [16]. In view of these facts, the electrical transport measurements are still challenging in the characterization of superconducting fullerenes. The zero-resistance state and Meissner effect on the same sample have only been realized recently for K- and Rb-doped C_{60} through the improvements of the sample quality and measurement techniques [25, 26].

It has been generally accepted that the resistivity measurement at required high magnetic field and low temperature is a reliable method for accurately determining the critical magnetic field which is fundamentally important due to its close relation to the coherent length and the Cooper pairing strength [28]. At the moment, the upper critical field $H_{c2}(0)$ values of K_3C_{60} were obtained either through the low-magnetic-field measurements of the magnetization [10, 29] and resistivity [17, 23, 30] or the high-magnetic-field non-contact measurements based on the ac magnetization [31–33] and radiofrequency technique [34, 35]. Having accurate $H_{c2}(0)$ of K_3C_{60} through the resistivity measurements at high enough magnetic

*Electronic address: xjchen2@gmail.com

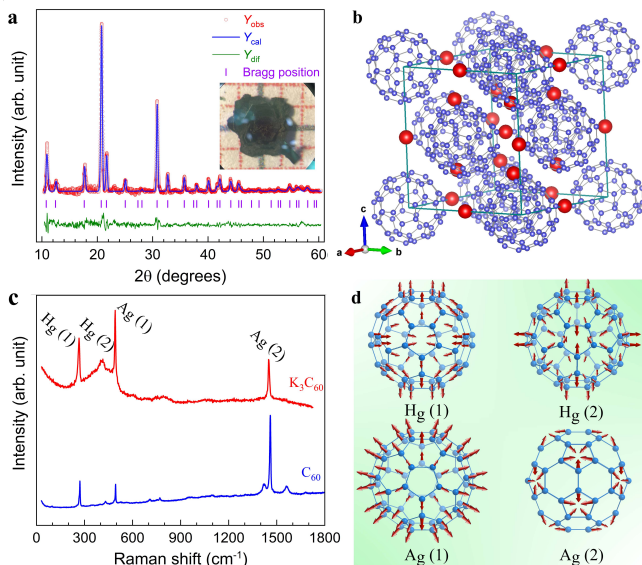


FIG. 1: Structural and spectroscopic characterizations of K-doped C_{60} . (a) Experimentally observed (red dots) and calculated (blue solid line) x-ray diffraction patterns for the doped sample at room temperature. The vertical purple lines present the Bragg reflection positions of the fcc structure, and the solid green line at the bottom represents the difference profile. Inset: Sample picture taken under microscope. (b) Crystal structure of fcc K_3C_{60} . The violet and red balls represent C and K atoms, respectively. (c) Raman scattering spectra of pure and K-doped C_{60} . (d) Schematic diagram of four representative intramolecular vibrational modes for K_3C_{60} . The red arrows indicate the vibrational directions of the C atoms.

fields is still highly desired. Here we choose K-doped C_{60} with the considerations of its similarity to other fullerenes [8, 14] and simplicity due to the absence of the antiferromagnetic state to solve this long-standing issue with the purpose to provide the constraints on the identification of the existing theoretical models or the future theory developments from a full set of superconducting parameters.

II. RESULTS

A. Crystal structure and molecular vibrations of K-doped C_{60}

Wet chemistry method was used to synthesize K-doped C_{60} detailed in Method. The quality, structure, and phase of the sample were examined by x-ray diffraction (XRD) and Raman scattering measurements. The XRD profile can be well indexed by the $Fm\bar{3}m$ space group [Fig. 1(a)], indicating that the synthesized K-doped C_{60} sample is a single-phase compound with the face-centered cubic (fcc) structure [Fig. 1(b)]. The obtained lattice parameter a is 14.22 ± 0.01 Å, in good agreement with those reported previously [11, 14].

Figure 1(c) shows Raman spectra of the pristine and

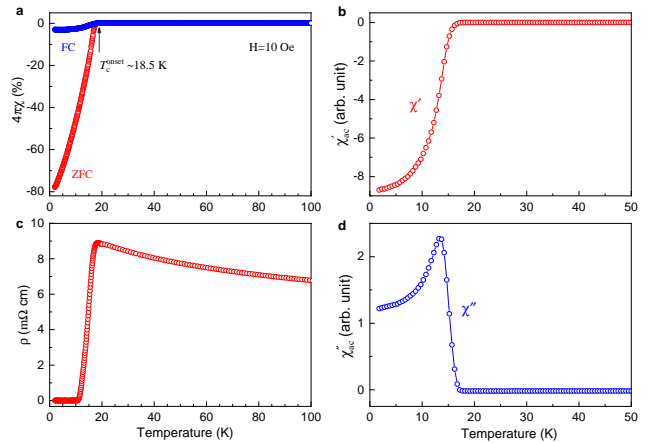


FIG. 2: Characterization of superconductivity of K_3C_{60} from the magnetic susceptibility and electrical transport measurements. (a) DC magnetic susceptibility (χ) with temperature range of 1.8-100 K at the applied magnetic field of 10 Oe. Zero-field-cooling (ZFC, red circles) and field-cooling (FC, blue circles) χ show an obvious diamagnetism below 19 K. (b) Real part of the ac magnetic susceptibility (χ'_{ac}) in the temperature range from 1.8 to 50 K. The probe harmonic magnetic field and frequency are 5 Oe and 234 Hz, respectively. (c) Temperature dependence of the electrical resistivity (ρ). (d) Imaginary component of the ac magnetic susceptibility (χ''_{ac}) as a function of temperature (1.8-50 K).

K-doped C_{60} collected at room temperature. All the Raman-active modes for C_{60} , including two A_g modes (at 497 and 1469 cm^{-1}) and eight H_g modes: 272, 432, 710, 772, 1100, 1248, 1422, and 1574 cm^{-1} , are observed in the pristine C_{60} , agreeing well with the literature [36]. The two low-frequency H_g modes and two A_g modes have strong intensities in K-doped C_{60} . The vibrations of these four modes [37] are shown schematically in Fig. 1(d). A recognized approach to determine the doping level of K_xC_{60} is the line-shift of the pinch mode $A_g(2)$. The observed 17 cm^{-1} redshift of this mode yields the doping concentration of about 3 estimated by the empirical relation of 6 cm^{-1} per elementary charge [38]. Therefore, the synthesized sample is homogeneous and has the chemical formula of K_3C_{60} with the fcc structure.

B. Superconductivity of K_3C_{60}

The superconductivity of the synthesized K_3C_{60} was identified by the existence of both the Meissner effect and zero resistance state. Figure 2 shows the results from the dc and ac susceptibility (χ) and resistivity measurements. The dc susceptibility directly demonstrates the Meissner effect of the sample, as shown in Fig. 2(a). Zero-field-cooling (ZFC) and field-cooling (FC) χ curves exhibit a clear drop below 18.5 K, which is defined as T_c . The shielding fraction (SF) of 80% at 2 K is estimated from the ZFC χ curve. This diamagnetic effect is also

observed through the real part (χ'_{ac}) of the ac susceptibility [Fig. 2(b)], similar to the ZFC χ curve from the dc measurement. As shown in Fig. 2(c), the resistivity drops rapidly below 18.7 K and quickly reaches the absolute zero value. The zero-resistivity transition of the sample is also indirectly reflected by the imaginary part (χ''_{ac}) of the ac susceptibility. To response the vortex current signal, χ''_{ac} can only be induced when the resistivity drops sharply because of the relatively large resistivity in the normal state and the flux exclusion in the complete Meissner state [39]. The peak shape of χ''_{ac} in Fig. 2(d) is the manifestation of the sharp drop in resistivity. As learned from the literature for the representative magnetization [1, 10–13, 32, 33] and nearly all electrical transport [1, 15, 17, 18, 20–23, 40, 41] measurements, the evidence for the zero-resistance state and the Meissner effect taken on the same K_3C_{60} sample is quite rare. The present study together with our recent efforts [25–27] provides solid experimental evidence for supporting superconductivity in synthesized fullerenes based on its two essential characters.

C. Upper critical field determined by resistivity measurements

Figure 3(a) shows the temperature dependence of the resistivity at low magnetic fields of 0–9 T. With increasing magnetic field, T_c shifts toward lower temperatures [Fig. 3(a)]. The resistivity behaviours at low temperatures and pulsed magnetic fields up to 50 T are given in Fig. 3(b). The determination of H_{c2} at a given temperature is illustrated in the inset of this figure. The $H_{c2}(T)$ data obtained from the high- and low-magnetic fields can be well described by the Werthamer-Helfand-Hohenberg theory [42]. Note that the experimentally observed H_{c2} 's at low temperatures are significantly larger than the orbital limit field $H_{c2}^{orb}(0)$ of 22 T estimated from the $H_{c2}(T)$ slope in the low-field regime ($H \leq 1$ T) by using $H_{c2}^{orb}(0) = 0.69 \times T_c \times |dH_{c2}/dT|_{T=T_c}$, suggesting the strong coupling effect. The experimentally obtained $H_{c2}(0)$ of 33.0 ± 0.5 T basically agrees with most of the high-field experimental results for this material [31, 32, 34, 35].

The reliability of the obtained $H_{c2}(0)$ value is guaranteed by the direct electrical transport measurements at enough high magnetic fields and at low temperatures. As a key indicator in the applications of superconducting materials, the $H_{c2}(0)$ of K_3C_{60} is little bit higher than that of Nb_3Sn with lower T_c of 18 K [43], a typical three-dimensional superconductor well known as superconducting magnets. Interestingly, our $H_{c2}(0)$ value for K_3C_{60} at ambient pressure is even comparable to those of fcc CeH_{10} with much higher $T_c = 115$ K at pressure of 95 GPa [44] and ThH_9 with $T_c = 151$ K at 170 GPa [45]. However, the need of high pressures to access the superconducting state in these superhydrides limits their technological applications. The larger $H_{c2}(0)$ for K_3C_{60}

with the higher T_c compared to those in Nb_3Sn offers the attractive opportunities for the technological applications due to the rich carbon abundance on the Earth as well as the low cost. Therefore, the present experimental finding opens a window for future developments and designs of the three-dimensional superconducting magnets based on this material.

D. Lower critical field, penetration depth, and coherence length

The obtained $H_{c2}(0)$, combined with other superconducting parameters such as the lower critical field H_{c1} , London penetration depth λ_L , and coherence length ξ , are crucial to the understanding of the physical properties and the mechanism of superconductivity of a type-II superconductor. The H_{c1} is determined by the magnetic-field dependence of the dc magnetization $M(H)$ at various temperatures below T_c [Fig. 3(c)]. Within this method, the magnetic field that initially deviates from the linear $M(H)$ behaviour is defined as $H_{c1}(T)$ for a given temperature, as illustrated in the upper right of Fig. 3(d). The $H_{c1}(T)$ values at different temperatures plotted in Fig. 3(d) are used to determine $H_{c1}(0)$ of 6.9 ± 0.1 mT through the empirical relation [28] $H_{c1}(T)/H_{c1}(0) = 1 - (T/T_c)^2$. With these critical fields, λ_L and the Ginzburg-Landau coherence length (ξ_{GL}) can be determined by using the equations: $H_{c2}(0) = \Phi_0/2\pi\xi_{GL}^2$ and $H_{c1}(0) = (\Phi_0/4\pi\lambda_L^2)\ln(\lambda_L/\xi_{GL})$ with the flux quantum $\Phi_0 = 2.0678 \times 10^{-15}$ Wb. We thus have $\lambda_L = 3325 \pm 36$ Å, $\xi_{GL} = 31.6 \pm 0.3$ Å, and the Ginzburg-Landau parameter $\kappa = \lambda_L/\xi_{GL} = 105 \pm 2$. These results are compared with those determined by using various techniques such as the magnetization [10, 29, 46, 47], magnetoresistance [23], muon spin relaxation [48, 49], nuclear magnetic resonance [50, 51], and optical reflectivity [24].

E. Determination of critical current density

Figure 3(e) displays the dc magnetic hysteresis loops at several fixed temperatures below T_c . With increasing temperature, the hysteresis loops gradually shrink inward until converting to a straight line near T_c . The diamond-like loop and temperature-dependent shrinkage are typical features for a type-II superconductor. The critical current density (J_c) can be determined simply from these dc magnetic loops based on Bean's critical state model [52] by using the formula $J_c = A \times (M_+ - M_-)/r$, where M_+ and M_- are the magnetizations in the decreasing and increasing circles at a given field H , and A and r are the shape of sample [53] and the sample radius, respectively. In our estimation, the radius r is assumed to be $1 \mu\text{m}$ according to the XRD results. The $J_c(H=0)$ variation with temperature is shown in Fig. 3(f). The obtained J_c value for K_3C_{60} in the present work differs largely with

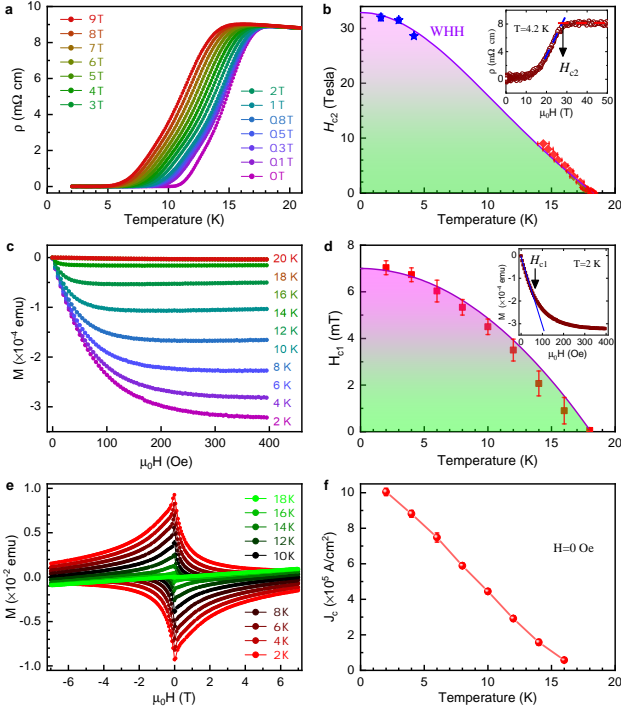


FIG. 3: Determination of superconducting parameters of K_3C_{60} . (a) Temperature-dependent resistivities at various magnetic fields up to 9 T. (b) Temperature dependence of the upper critical field $H_{c2}(T)$. The data points of the red diamonds and blue pentacles are obtained from the electrical transport measurements based on the fixed-field (a) and fixed-temperature scans, respectively. Error bars represent estimated uncertainties in determining H_{c2} . The solid line is the fitting to the Werthamer-Helfand-Hohenberg theory. Inset: Magnetic field dependent resistivity with scanning field up to 50 T at temperature of 4.2 K. H_{c2} for a fixed temperature is determined from the intercept of the linear extrapolations from below and above the transition. (c) Magnetic-field dependence of the magnetization (M) at various temperatures. (d) Temperature dependence of the lower critical field $H_{c1}(T)$. The solid curve is the fitting of the measured data points to the empirical law $H_{c1}(T)/H_{c1}(0) = 1 - (T/T_c)^2$. Inset: The magnetization as a function of magnetic field at 2 K. The derivation from the initial linear trend is used for the determination of H_{c1} . (e) Magnetic hysteresis (M - H) loops at various temperatures with the applied field up to ± 7 T. (f) Temperature dependence of the critical current density (J_c). The J_c value is determined from the M - H loop (e) based on the Bean's critical-state model.

the early results obtained from the same magnetization measurements [10, 20, 29, 33, 47, 54–57]. The difference mainly comes from the uncertainties for the radius r , which has been confirmed by the functional relationship between J_c and the particle size [54]. Meanwhile, the granularity of the sample also affects the J_c value [29].

It should be emphasized that J_c is important for evaluating technological applications of a superconductor. The material itself possesses a self-field component $J_c(s)$

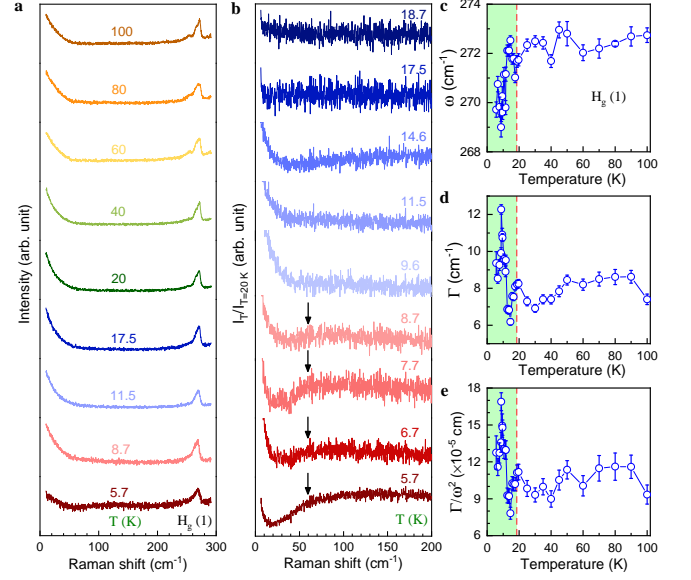


FIG. 4: Raman spectra in the low-frequency region of K_3C_{60} . (a) Raman spectra at several representative temperatures before and after the superconducting transition. The scattering peak at around 270 cm^{-1} is assigned as the $H_g(1)$ mode. (b) Raman spectra normalized by the intensity at 20 K. The intensity shows a linear decrease below 60 cm^{-1} (as marked by the arrows) when the temperature is lower than $1/2 T_c$, and it becomes more obvious at lower temperatures. (c-e) Temperature dependence of the frequency (ω), linewidth (Γ), and electron-phonon coupling parameter Γ/ω^2 of the $H_g(1)$ mode, from top to bottom, respectively. Green shadow areas represent the superconducting state.

even without applying external field. For a type-II superconductor, $J_c(s)$ follows a universal expression [58] $J_c(s) = H_{c1}/\lambda_L$. It is clear that $J_c(s)$ is independent of the material geometry. Substituting the obtained H_{c1} and λ_L , we have $J_c(s)$ of $1.7 \times 10^6\text{ A/cm}^2$ for K_3C_{60} , slightly larger than $J_c(H=0)$ determined from the magnetization measurements [Figs. 3(e)-3(f)]. Therefore, the technological parameters of T_c , H_{c2} , and J_c needed for K_3C_{60} to function as a superconducting magnet material are well established.

F. Detection of superconducting gap and evaluation of electron-phonon coupling

The superconducting energy gap (Δ) of K_3C_{60} is determined based on the Raman spectroscopy measurements. Figure 4(a) shows the representative Raman spectra in the low-frequency region at a wide temperature range from 5.7 to 100 K. In Fig. 4(b), the Raman spectra at low temperatures below T_c were normalized by dividing the spectrum measured at temperature of 20 K. One can see clearly a linear decrease in the scattering intensity below 60 cm^{-1} (as marked by arrows) when the temperature cools down to $1/2 T_c$. This feature becomes

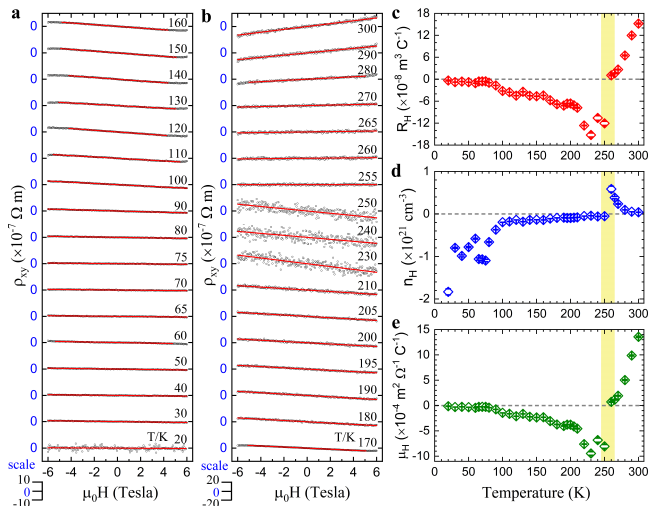


FIG. 5: Hall effect data of K_3C_{60} . Hall resistivity (ρ_{xy}) vs. the applied magnetic field along the two opposite directions up to 6 T in the temperature range from 20 to 160 K (a) and from 170 to 300 K (b). Numerical scale is given in the left bottom. The Hall coefficient (R_H) (c) carrier concentration (n_H) (d) and mobility (μ_H) (e) as a function of temperature. The yellow regions in (c-e) denote the boundary for the occurrence of the orientational transition.

more obvious at lower temperatures. Such a linear decrease in the intensity of the electronic scattering can be attributed to the renormalization of the density of state due to the superconducting transition [59]. The 2Δ value can be taken from the position where the frequency starts to deviate the linear behaviour. The reduced energy gap $2\Delta/k_B T_c$ of 4.7 ± 0.3 is thus obtained with k_B being the Boltzmann constant. This value is higher than 3.53 predicted within the BCS framework. The high $2\Delta/k_B T_c$ and large $H_{c2}(0)$ together indicate the strong coupling of the interactions in this superconductor. Similar conclusions have also been drawn from other techniques including point-contact tunneling spectroscopy [60, 61] and nuclear magnetic resonance [62]. Some other studies based on the optical reflectivity [24, 63], nuclear magnetic resonance [50, 62], and photoemission [41] support weak electron-phonon coupling within the conventional BCS framework.

For type-II spin-singlet superconductors, the orbital and Pauli paramagnetic effects are two distinct ways for pair-breaking with increasing external magnetic field. Using $2\Delta/k_B T_c = 4.7 \pm 0.3$, the Pauli-limiting field $H_P = 45.4 \pm 2.2$ T is then determined accurately from $H_P = \Delta/(\sqrt{2}\mu_B)$ [64] with μ_B being the Bohr magneton. The obtained orbital component of the upper critical field H_{c2}^{orb} of 22 T is much smaller than H_P , yielding the Maki parameter [65] $\gamma = \sqrt{2}H_{c2}^{orb}/H_P \sim 0.7$. Since γ reflects the strength of the paramagnetic effect, this indicates that the orbital effect dominates the H_{c2} behaviour for this superconductor.

In addition, the electron-phonon contribution to the

TABLE I: Summary of the superconducting parameters of K_3C_{60} .

T_c (K)	18.5 ± 0.5
$H_{c1}(0)$ (mT)	6.9 ± 0.1
$H_{c2}(0)$ (T)	33.0 ± 0.5
λ_L (\AA)	3325 ± 36
ξ_{GL} (\AA)	31.6 ± 0.3
J_c ($\times 10^4$ A/cm 2)	100 ± 2
$2\Delta/k_B T_c$	4.7 ± 0.3
v_F ($\times 10^4$ m/s)	5.6 ± 0.4
E_F (meV)	55 ± 13
T_F (K)	641 ± 147

superconductivity can be evaluated from the observations of the Raman spectra at temperatures below T_c . The low-frequency $H_g(1)$ intramolecular vibrational mode is chosen as an example to monitor the superconductivity-induced changes. The systematic change of this mode can be seen from Fig. 4(a). The temperature dependence of the frequency (ω), linewidth (Γ), and electron-phonon coupling parameter Γ/ω^2 of this $H_g(1)$ mode is shown in Figs. 4(c)-4(e), from top to bottom, respectively. When entering the superconducting state (the green shaded zone), the $H_g(1)$ mode exhibits the downshift (softening) in ω , the increase (widening) in Γ , and the enhancement of Γ/ω^2 . These behaviours are due to the superconductivity-induced phonon self-energy effect. The early proposal [66] regarding the phonon evolution with temperature when this material enters the superconducting state with high-resolution from an inelastic scattering technique is finally realized here. The absence of phonon mode near 40 cm^{-1} in the Raman spectra at temperatures below T_c indicates that it is probably an acoustic branch and thus inactive to Raman scattering but visible in the neutron measurements [66]. These results provide the strong support for the important contribution of the electron-phonon coupling to the superconductivity in K_3C_{60} . The observed self-energy effect together with the large $2\Delta/k_B T_c$ obtained from the same Raman spectra reveals the strong electron-phonon coupling in K_3C_{60} , which needs to be included in dealing with the phonon effects [67–73].

G. Determination of Hall coefficient

The magnetic-field-dependent Hall resistivities of K_3C_{60} with applied magnetic fields up to ± 6 T at various temperatures from 20 to 300 K are shown in Figs. 5(a) and 5(b). The Hall resistivity ρ_{xy} versus H curves at all studied temperatures are essentially linear, ensuring the accurate determination of the Hall coefficient R_H through the linear fitting to the data points [Fig. 5(c)]. The carrier concentration n_H and mobility μ_H are thus obtained through $n_H = 1/(eR_H)$ and $\mu_H = \sigma_{xx} R_H$ with e

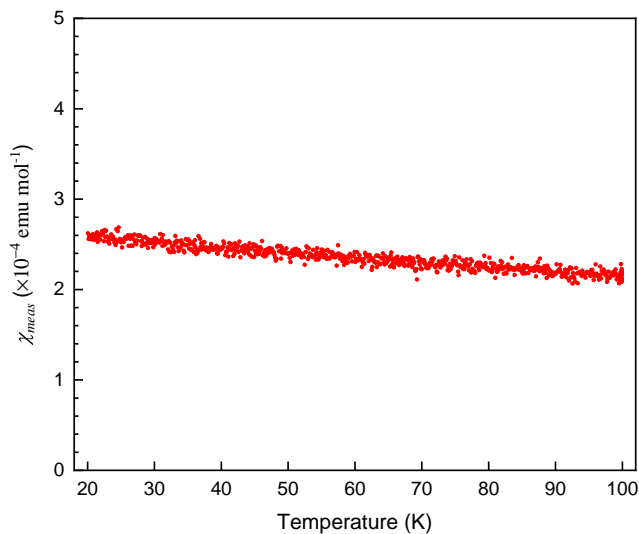


FIG. 6: Magnetic susceptibility χ_{meas} of K_3C_{60} in the temperature range of 20-100 K.

and σ_{xx} being the electron charge and the electrical conductivity, respectively [Figs. 5(d)-5(e)]. As can be seen, R_H changes sign at the temperature range of 220-250 K. The change of the carrier character further indicates that the synthesized sample is in a half-filled state with both electron and hole conduction [17, 74]. Similar sign change has also been observed in K_3C_{60} thin films [17] but was absent in the study for K- and Rb-doped C_{60} single crystals [75]. Interestingly, around the temperature for the sign change, the orientational ordering transition has been reported for C_{60} [76] and K_3C_{60} [25, 77]. The Hall effect clearly captures the effect of the orientational ordering on the electronic structure. Most importantly, the obtained evolution of n_H with temperature close to T_c not only gives the accurate carrier concentration for K_3C_{60} to superconduct but also determines the electronic feature at low temperatures rather than the hole character at room temperature, though the two carrier behaviour was noticed in the band structure calculations [74] and the electron doping is generally believed.

H. Full set of superconducting parameters

Table I summarizes the obtained superconducting parameters for K_3C_{60} . These parameters obtained from the same sample could settle down the large contradictions from different groups. For instance, the reported $H_{c1}(0)$ values in the literature are in the range from 1 to 13 mT with the difference in one order of magnitude [10, 29, 47, 78]. Our $H_{c1}(0)$ value locates in the middle of this range. In the case of $2\Delta/k_B T_c$, the early results are in the range of 3-3.6 revealed by far-infrared the optical reflectivity [24, 63], nuclear magnetic resonance [50, 62], and photoemission [41], suggestive of the weak BCS cou-

pling. Meanwhile, the strong coupling effect is supported by the large $2\Delta/k_B T_c$ values from 4.3 to 6 based on the scanning tunneling microscopy [60, 61] and nuclear magnetic resonance [62] measurements. The obtained value of 4.7 ± 0.3 for K_3C_{60} from the present work is in the middle range of these studies, which supports the strong coupling effect.

Having the knowledge of ξ_{GL} based on the well determined $H_{c2}(0)$ as well as Δ , one can derive the average Fermi velocity v_F of $(5.6 \pm 0.4) \times 10^4$ m/s by using the formula $v_F = \pi \Delta \xi_{GL} / \hbar$, in good agreement with the measurements and calculations [46, 74]. The measured magnetic susceptibility χ_{meas} (Fig. 6) at 20 K gives the Pauli susceptibility $\chi_{spin} = (7.5 \pm 0.6) \times 10^{-4}$ emu/mol after the correction of the core and Landau diamagnetic contributions. Taking the n_H value at 20 K (Fig. 5) for the conduction electron density n , we obtain the effective mass $m^* = (6.2 \pm 0.6)m_0$ from the expression $\chi_{spin} = \mu_B m^* (3\pi^2 n)^{1/3} / \hbar^2 \pi^2$, where m_0 and \hbar are the mass of the free electron and the reduced Planck constant, respectively. The result for m^* is very close to $(6.4 \pm 1.5)m_0$ in the early study [46]. Using the v_F and m^* value, we have $E_F = 55 \pm 13$ meV and the Fermi temperature $T_F = 641 \pm 147$ K for K_3C_{60} based on the formula $E_F = m^* v_F^2 / 2 = k_B T_F$. Note that all these important parameters are obtained on the same sample in terms of the generally accepted techniques. Table I is thus updated to include them.

III. DISCUSSION AND CONCLUSIONS

It was often expected to elucidate the driving force for superconductivity from the isotope effect. However, the existing isotope exponent α deviates the predicted value of 0.5 from the BCS theory and can be divided into two groups depending on the ^{13}C enrichment, one [79] with $\alpha < 0.5$ and the other [80–82] with $\alpha > 1.0$. The former suggests the strong coupling effect, consistent with our Raman data, and the latter favors the electron correlations [83, 84]. Therefore, the isotope effect suggests that the superconducting pairing in K_3C_{60} originates from either the strong electron-phonon interaction or the electronic correlations. However, it is hard to pin down the exact mechanism due to the scatter of the data.

Now that a full set of parameters for K_3C_{60} (Table I) has been obtained from the same sample at all the necessary measurement conditions and techniques, they should provide the reliable constraints on the examination of the existing theories and the future theory development for the mechanism of superconductivity. The determined $H_{c2}(0)$ not only yields ξ_{GL} and but also further gives v_F with the help of Δ . The magnetization and Hall effect data give m^* and thus T_F when combining v_F . These self-consistently obtained parameters along with T_c at least can be used to see how far away or close the studied K_3C_{60} locates to the well known superconductors.

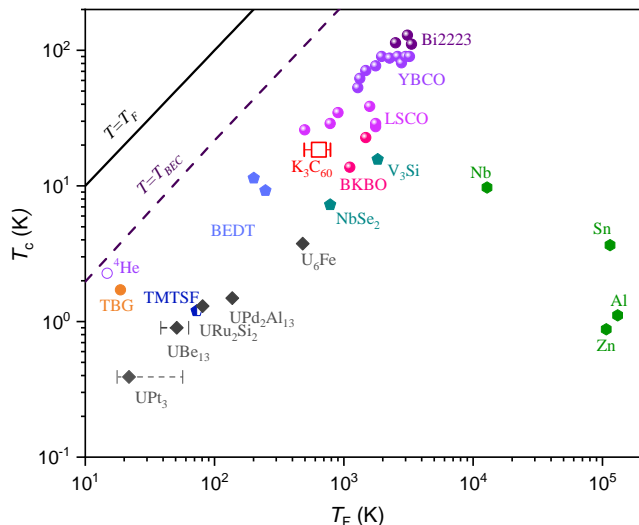


FIG. 7: Relationship between the critical temperature T_c and the Fermi temperature T_F of representative superconductors. The data derived from the current measurements for K_3C_{60} (open square) are compared with those of various superconductors taken from the previous works [7, 86]. Bi2223, YBCO, LSCO, and BKBO represent $Bi_2Sr_2(Ca,Pb)_2Cu_3O_{10+\delta}$, $YBa_2Cu_3O_{7-\delta}$, $La_{2-x}Sr_xCuO_4$, and $Ba_{1-x}K_xBiO_3$, respectively. TMTSF and BEDT are two organic charge-transfer salts. TBG denotes twisted bilayer graphene. The broken line denotes the Bose-Einstein condensation temperature T_{BEC} for an ideal three-dimensional boson gas.

A recognized measure for judging the nature of correlated superconductors is through the change trend for T_c and T_F . All the reported correlated superconductors discovered so far including cuprates, heavy fermion systems, organic materials [85, 86], and even twisted graphene [7] follow a linear relationship between T_c and T_F . The common characters for these superconductors are the existence of some competing order(s) and the strong electron correlation effect. Thus, the electron correlations are believed to be the major player for superconductivity in these systems. When adding the obtained T_c and T_F values for K_3C_{60} in the map (Fig. 7), we find that this superconductor nicely follows the same linear trend as the other correlated superconductors but being very close to $Ba_{1-x}K_xBiO_3$. The trend itself classifies K_3C_{60} as an unconventional correlated superconductor. The neighbourhood for $Ba_{1-x}K_xBiO_3$ and K_3C_{60} implies that their superconductivity may be governed by the similar factors. For $Ba_{1-x}K_xBiO_3$, till recently it was found [87] that the electron correlations enhance the electron-phonon coupling and they together contribute to the high T_c in this system. It is reasonable to believe both the electron correlations and electron-phonon coupling jointly account for superconductivity in K_3C_{60} . This idea finds the support from the theoretical calculations on alkali-doped fullerenes mainly focusing on Cs_3C_{60} [72],

where the electron-phonon coupling was found to enhance the electron correlations and they together gave the correct T_c evolution trend with the unit cell volume, though the calculated T_c is generally lower about 10 K than the experimental value. Since the strong coupling effect in K_3C_{60} has been firmly established from high T_c , high $H_{c2}(0)$, large $2\Delta/k_B T_c$, and the Raman data, the T_c and T_F relation derived from other parameters further suggests unconventional correlated superconductivity and the joint contributions from the electron-phonon coupling and electron correlations [8, 9]. Recalling the unconventional isotope effect, the nice collaboration between the strong electron-phonon coupling and electron correlations is thus suggested to be responsible for the observed unconventional superconductivity in K_3C_{60} , both in a favorable way. This should be the base and constraints on the examinations of the existing theories and the future theory development for the mechanism of superconductivity for fullerenes.

IV. EXPERIMENTAL DETAILS

Sample synthesis. High-quality K-doped C_{60} sample was synthesized by using a modified version of a solution-phase reaction process detailed previously [12, 25, 26]. High-purity potassium (99%, Sinopharm Chemical Reagent) and fullerene powder (99.9%, Acros Organics) were mixed with the nominal mole ratio of 3:1 (K: C_{60}). The mixtures, together with certain dose of ultra-dry tetrahydrofuran (THF) solvent, were loaded into a 15 ml borosilicate vial. The glass vial was then treated in an ultrasonic device at around 50 °C for 5-10 minutes to accelerate the dissolution of alkali metals and the reaction between potassium and C_{60} molecules. The colour of the solution turned reddish-brown after the ultrasound process. It should be noted that the temperature of the reaction can not exceed 63 °C, which is the melting point of potassium, otherwise potassium would melt into small spheres that are difficult to react, thus breaking the desired stoichiometric ratio for superconducting phase. After that, the solution was oscillated in a vortex mixer (Vortex 3000, Wiggins) with 200 r/min for 10 hours to ensure the complete reaction and the homogeneity of sample. Upon filtering, we obtained a black preliminary product. All the above preparation steps were carried out in an argon-filled glovebox with both O_2 and H_2O levels less than 0.1 ppm. The as-prepared K_3C_{60} was then put into quartz tubes and sealed under vacuum about 1×10^{-4} Pa. The fragile K_3C_{60} sample was obtained after annealing at 250 °C for 20 hours.

Characterization of crystal structure. The crystal structure was determined based on the X-ray diffraction spectrometer (Panalytical Emperean) by using Cu K_α radiation with wavelength of 1.5406 Å. The polyimide film was used to cover the sample to avoid the oxidation of K_3C_{60} . The background signals of the film were carefully subtracted in the subsequent analysis. The space

group and lattice parameters were determined by using *Jana 2020* program [88] based on the Le Bail method [89] to fit the diffraction patterns.

Raman spectroscopy measurements. The Raman spectra were collected in an in-house system with Charge Coupled Device and Spectrometer from Princeton Instruments. The laser with the wavelength of 488 nm and power less than 2 mW was used in the measurements. Pristine and doped C_{60} were sealed in capillary tubes when collecting the Raman spectra at room temperature [Fig. 1(c)]. For cryogenic Raman spectroscopy experiment, the doped sample was loaded into a sealed cooper holder with an optical quartz window. The sample was then put on the holder equipped with a heater in a cryogenic vacuum chamber to obtain the temperature-dependent Raman spectra (Fig. 4).

Magnetization measurements. The magnetization measurements were carried out by using a Magnetic Properties Measurement System (MPMS3, Quantum Design). The sample was placed into a nonmagnetic capsule and sealed by GE Varnish to protect K_3C_{60} from air. The *dc* magnetic susceptibility $\chi(T)$ curves were collected with the ZFC and FC runs at the field of 10 Oe at temperature ranging from 1.8 to 100 K. In the *ac* magnetic susceptibility measurements, the used probe harmonic magnetic field and frequency are 5 Oe and 234 Hz, respectively. The $M(H)$ plots at various fixed temperatures were collected by two steps. Firstly, the step-size was set to 5 Oe in stable mode from 0 to 400 Oe. Secondly, the H swept from +7 T to -7 T, and then went back to get the complete hysteresis loop.

Pauli (spin) susceptibility χ_{spin} . The measured magnetic susceptibility χ_{meas} is determined by the sum of the paramagnetic (χ_P) and diamagnetic (χ_D) components. The χ_D component includes the core and/or conduction electron (Landau) contributions, where the former can be estimated based on the pub-

lished Pascal constants, and the latter usually takes 1/3 for the paramagnetic term. The value of χ_D for K_3C_{60} can be calculated by $\chi_D(K_3C_{60})=60\chi_D(C\text{ atom})+3\chi_D(K\text{ atom})+\chi_{Landau}(\text{conduction electron})$, in which $\chi_D(C\text{ atom})=-6.0\times 10^{-6}$ emu/mol and $\chi_D(K\text{ atom})=-18.5\times 10^{-6}$ emu/mol. We thus obtain $\chi_D=-(5.0\pm 0.3)\times 10^{-4}$ emu/mol. By using $\chi_{meas}=(2.5\pm 0.3)\times 10^{-4}$ emu/mol at 20 K (Fig. 6), we have the total bulk paramagnetic susceptibility $\chi_P=(7.5\pm 0.6)\times 10^{-4}$ emu/mol, which can be taken as the Pauli paramagnetic susceptibility χ_{spin} .

Resistivity and Hall effect measurements. Due to the high sensitivity of the sample to air, a nonmagnetic Ni-Cr-Al alloy cell equipped with four air-tight copper leads was developed to measure the electrical and Hall resistivities when keeping good contact between sample and four electrodes and avoiding oxidation. The resistivity and Hall coefficient were determined in terms of the van der Pauw method [90]. The sample thickness for the electrical transport measurements is 0.2 mm. The low-field resistivity and Hall effect measurements were performed on Physical Property Measurement System (Quantum Design, PPMS). The resistivities at paused magnetic fields up to 50 T with the help of a typical four-contact method were measured at the National High Magnetic Field Center, Wuhan, China.

Acknowledgements

This work was supported from the Shenzhen Science and Technology Program (Grant No. KQTD20200820113045081), the Basic Research Program of Shenzhen (Grant No. JCYJ20200109112810241), and the National Key R&D Program of China (Grant No. 2018YFA0305900).

-
- [1] A.F. Hebard, M.J. Rosseinsky, R.C. Haddon, D.W. Murphy, S.H. Glarum, T.T.M. Palstra, A.P. Ramirez, and A.R. Kortan, *Superconductivity at 18 K in potassium-doped C_{60}* , Nature **350**, 600 (1991).
 - [2] M.J. Rosseinsky, A.P. Ramirez, S.H. Glarum, D.W. Murphy, R.C. Haddon, A.F. Hebard, T.T.M. Palstra, A.R. Kortan, S.M. Zahurak, and A.V. Makhija, *Superconductivity at 28 K in Rb_xC_{60}* , Phys. Rev. Lett. **66**, 2830 (1991).
 - [3] T.T.M. Palstra, O. Zhou, Y. Iwasa, P.E. Sulewski, R.M. Fleming, and B.R. Zegarski, *Superconductivity at 40 K in cesium doped C_{60}* , Solid State Commun. **93**, 327 (1995).
 - [4] Y. Takabayashi, A.Y. Ganin, P. Jeglič, D. Arčon, T. Takano, Y. Iwasa, Y. Ohishi, M. Takata, N. Takeshita, K. Prassides *et al.*, *The disorder-free non-BCS superconductor Cs_3C_{60} emerges from an antiferromagnetic insulator parent state*, Science **323**, 1585 (2009).
 - [5] A.Y. Ganin, Y. Takabayashi, P. Jeglič, D. Arčon, A. Potočnik, P.J. Baker, Y. Ohishi, M.T. McDonald, M.D. Tzirakis, A. McLennan *et al.*, *Polymorphism control of superconductivity and magnetism in Cs_3C_{60} close to the Mott transition*, Nature **466**, 221 (2010).
 - [6] H.W. Kroto, J.R. Heath, S.C. O'Brien, R.F. Curl, and R.E. Smalley, *C_{60} : Buckminsterfullerene*, Nature **318**, 162 (1985).
 - [7] Y. Cao, V. Fatemi, S. Fang, K. Watanabe, T. Taniguchi, E. Kaxiras, and P. Jarillo-Herrero, *Unconventional superconductivity in magic-angle graphene superlattices*, Nature **556**, 43 (2018).
 - [8] O. Gunnarsson, *Superconductivity in fullerides*, Rev. Mod. Phys. **69**, 575 (1997).
 - [9] M. Capone, M. Fabrizio, C. Castellani, and E. Tosatti, *Colloquium: Modeling the unconventional superconducting properties of expanded A_3C_{60} fullerides*, Rev. Mod. Phys. **81**, 943 (2009).
 - [10] K. Holzer, O. Klein, G. Grüner, J.D. Thompson, F. Diederich, and R.L. Whetten, *Critical magnetic fields in the superconducting state of K_3C_{60}* , Phys. Rev. Lett. **67**,

- 271 (1991).
- [11] P.W. Stephens, L. Mihaly, P.L. Lee, R.L. Whetten, S.-M. Huang, R.B. Kaner, F. Diederich, and K. Holczer, *Structure of single-phase superconducting K_3C_{60}* , *Nature* **351**, 632 (1991).
- [12] T. Yoon, J.Y. Koo, and H.C. Choi, *High yield organic superconductors via solution-phase alkali metal doping at room temperature*, *Nano Lett.* **20**, 612 (2020).
- [13] K. Holczer, O. Klein, S.-M. Huang, R.B. Kaner, K.-J. Fu, R.L. Whetten, and F. Diederich, *Alkali-fulleride superconductors: synthesis, composition, and diamagnetic shielding*, *Science* **252**, 1154 (1991).
- [14] R.M. Fleming, A.P. Ramirez, M.J. Rosseinsky, D.W. Murphy, R.C. Haddon, S.M. Zahurak, and A.V. Makhija, *Relation of structure and superconducting transition temperatures in A_3C_{60}* , *Nature* **352**, 787 (1991).
- [15] X.-D. Xiang, J.G. Hou, G. Briceño, W.A. Vareka, R. Mostovoy, A. Zettl, V.H. Crespi, and M.L. Cohen, *Synthesis and electronic transport of single crystal K_3C_{60}* , *Science* **256**, 1190 (1992).
- [16] O. Klein, G. Grüner, S.-M. Huang, J.B. Wiley, and R.B. Kaner, *Electrical resistivity of K_3C_{60}* , *Phys. Rev. B* **46**, 11247 (1992).
- [17] T.T.M. Palstra, R.C. Haddon, A.F. Hebard, and J. Zaanen, *Electronic transport properties of K_3C_{60} films*, *Phys. Rev. Lett.* **68**, 1054 (1992).
- [18] T.T.M. Palstra, A.F. Hebard, R.C. Haddon, and P.B. Littlewood, *Fermi-liquid behavior in the electrical resistivity of K_3C_{60} and Rb_3C_{60}* , *Phys. Rev. B* **50**, 3462 (1994).
- [19] R.C. Haddon, *Electronic structure, conductivity, and superconductivity of alkali metal doped C_{60}* , *Acc. Chem. Res.* **25**, 127 (1992).
- [20] W.B. Zhao, X.D. Zhang, Z.Y. Ye, J.L. Zhang, C.Y. Li, D.L. Yin, Z.N. Gu, X.H. Zhou, and Z.X. Jin, *Synthesis of K_3C_{60} single crystal thin films with high critical currents*, *Solid State Commun.* **85**, 945 (1993).
- [21] Y. Maruyama, T. Inabe, H. Ogata, Y. Achiba, S. Suzuki, K. Kikuchi, and I. Ikemoto, *Observation of metallic conductivity and sharp superconducting transition at 19 K in potassium-doped fulleride C_{60} single crystal*, *Chem. Lett.* **20**, 1849 (1991).
- [22] X.-D. Xiang, J.G. Hou, V.H. Crespi, A. Zettl, and M.L. Cohen, *Three-dimensional fluctuation conductivity in superconducting single crystal K_3C_{60} and Rb_3C_{60}* , *Nature* **361**, 54 (1993).
- [23] J.G. Hou, V.H. Crespi, X.-D. Xiang, W.A. Vareka, G. Briceño, A. Zettl, and M.L. Cohen, *Determination of superconducting and normal state parameters of single crystal K_3C_{60}* , *Solid State Commun.* **86**, 643 (1993).
- [24] L. Degiorgi, P. Wachter, G. Grüner, S.-M. Huang, J. Wiley, and R.B. Kaner, *Optical response of the superconducting state of K_3C_{60} and Rb_3C_{60}* , *Phys. Rev. Lett.* **69**, 2987 (1992).
- [25] R.S. Wang, D. Peng, J.W. Hu, L.N. Zong, and X.J. Chen, *Oriental ordering and electron-phonon interaction in K_3C_{60} superconductor*, *Carbon* **195**, 1 (2022).
- [26] L.N. Zong, R.S. Wang, D. Peng, and X.J. Chen, *Superconductivity in nonstoichiometric rubidium-doped C_{60}* , *J. Phys. Chem. C* **126**, 2912 (2022).
- [27] R.S. Wang, D. Peng, L.N. Zong, L.C. Chen, and X.J. Chen, *Variation of the critical temperature with the lattice parameter in K_3C_{60}* , *Carbon* (<https://doi.org/10.1016/j.carbon.2022.07.070>) (2022).
- [28] M. Tinkham, *Introduction to superconductivity*, (McGraw-Hill, New York, 1975).
- [29] V. Buntar, F.M. Sauerzopf, H.W. Weber, J.E. Fischer, H. Kuzmany, and M. Haluska, *Mixed-state parameters and vortex pinning in single-crystalline K_3C_{60} fullerene superconductors*, *Phys. Rev. B* **56**, 14128 (1997).
- [30] J.G. Hou, X.-D. Xiang, M.L. Cohen, and A. Zettl, *Granularity and upper critical fields in K_3C_{60}* , *Physica C* **232**, 22 (1994).
- [31] C.E. Johnson, H.W. Jiang, K. Holczer, R.B. Kaner, R.L. Whetten, and F. Diederich, *Upper-critical-field-temperature phase diagram of alkali-metal-intercalated C_{60} superconductors*, *Phys. Rev. B* **46**, 5880 (1992).
- [32] G.S. Boebinger, T.T.M. Palstra, A. Passner, M.J. Rosseinsky, D.W. Murphy, and I.I. Mazin, *Evidence of upper-critical-field enhancement in K_3C_{60} powders*, *Phys. Rev. B* **46**, 5876 (1992).
- [33] M. Baenitz, M. Heinze, E. Straube, H. Werner, R. Schlögl, V. Thommen, H.-J. Güntherodt, and K. Lüders, *Inter- and intragrain AC response of the granular superconductors K_3C_{60} and Rb_3C_{60}* , *Physica C* **228**, 181 (1994).
- [34] S. Foner, E.J. McNiff, Jr., D. Heiman, S.-M. Huang, and R.B. Kaner, *Measurements of the upper critical field of K_3C_{60} and Rb_3C_{60} powders to 60 T*, *Phys. Rev. B* **46**, 14936 (1992).
- [35] Y. Kasahara, Y. Takeuchi, R.H. Zadik, Y. Takabayashi, R.H. Colman, R.D. McDonald, M.J. Rosseinsky, K. Prasad, and Y. Iwasa, *Upper critical field reaches 90 tesla near the Mott transition in fulleride superconductors*, *Nat. Commun.* **8**, 11467 (2017).
- [36] P. Zhou, K.A. Wang, Y. Wang, P.C. Eklund, M.S. Dresselhaus, G. Dresselhaus, and R.A. Jishi, *Raman scattering in C_{60} and alkali-metal-saturated C_{60}* , *Phys. Rev. B* **46**, 2595 (1992).
- [37] M. Schlüter, M. Lannoo, M. Needels, G.A. Baraff, and D. Tomanek, *Superconductivity in alkali intercalated C_{60}* , *J. Phys. Chem. Solids* **53**, 1473 (1992).
- [38] R.C. Haddon, A.F. Hebard, M.J. Rosseinsky, D.W. Murphy, S.J. Dulcos, K.B. Lyons, B. Miller, J.M. Rosamilia, R.M. Fleming, A.R. Kortan *et al.*, *Conducting films of C_{60} and C_{70} by alkali-metal doping*, *Nature* **350**, 320 (1991).
- [39] F. Gömöry, *Characterization of high-temperature superconductors by ac susceptibility measurements*, *Supercond. Sci. Technol.* **10**, 523 (1997).
- [40] A. Ugawa and K. Yakushi, *Infrared and transport properties of K_3C_{60}* , *Synthetic Met.* **55-57**, 2997 (1993).
- [41] R. Hesper, L.H. Tjeng, A. Heeres, and G.A. Sawatzky, *BCS-like density of states in superconducting A_3C_{60} surfaces*, *Phys. Rev. Lett.* **85**, 1970 (2000).
- [42] N.R. Werthamer, E. Helfand, and P.C. Hohenberg, *Temperature and purity dependence of the superconducting critical field, H_{c2} . III. Electron spin and spin-orbit effects*, *Phys. Rev.* **147**, 295 (1966).
- [43] A. Godeke, M.C. Jewell, C.M. Fischer, A.A. Squitieri, P.J. Lee, and D.C. Larbalestier, *The upper critical field of filamentary Nb_3Sn conductors*, *J. Appl. Phys.* **97**, 093909 (2005).
- [44] W. Chen, D.V. Semenov, X. Huang, H. Shu, X. Li, D. Duan, T. Cui, and A.R. Oganov, *High-temperature superconducting phases in cerium superhydride with a T_c up to 115 K below a pressure of 1 megabar*, *Phys. Rev. Lett.* **127**, 117001 (2021).

- [45] D.V. Semenov, A.G. Kvashnin, A.G. Ivanova, V. Svitlyk, V.Y. Fomin, A.V. Sadakov, O.A. Sobolevskiy, V.M. Pudalov, I.A. Troyan, and A.R. Oganov, *Superconductivity at 161 K in thorium hydride ThH₁₀: Synthesis and properties*, Mater. Today **33**, 36 (2020).
- [46] W.H. Wong, M.E. Hanson, W.G. Clark, G. Grüner, J.D. Thompson, R.L. Whetten, S.-M. Huang, R.B. Kaner, F. Diederich, P. Petit *et al.*, *Normal-state magnetic properties of K₃C₆₀*, Europhys. Lett. **18**, 79 (1992).
- [47] S.H. Irons, J.Z. Liu, P. Klavins, and R.N. Shelton, *Magnetic properties of superconducting K₃C₆₀ and Rb₃C₆₀ synthesized from large single-crystal fullerenes*, Phys. Rev. B **52**, 15517 (1995).
- [48] Y.J. Uemura, A. Keren, L.P. Le, G.M. Luke, B.J. Sternlieb, W.D. Wu, J.H. Brewer, R.L. Whetten, S.M. Huang, S. Lin *et al.*, *Magnetic-field penetration depth in K₃C₆₀ measured by muon spin relaxation*, Nature **352**, 605 (1991).
- [49] Y.J. Uemura, A. Keren, L.P. Le, G.M. Luke, W.D. Wu, J.S. Tsai, K. Tanigaki, K. Holczer, S. Donovan, and R.L. Whetten, *System dependence of the magnetic-field penetration depth in C₆₀ superconductors*, Physica C **235-240**, 2501 (1994).
- [50] R. Tycko, G. Dabbagh, M.J. Rosseinsky, D.W. Murphy, A.P. Ramirez, and R.M. Fleming, *Electronic properties of normal and superconducting alkali fullerenes probed by ¹³C nuclear magnetic resonance*, Phys. Rev. Lett. **68**, 1912 (1992).
- [51] S. Sasaki and C.W. Chu, *¹³C NMR observation of extreme type-II superconductivity in K₃C₆₀: A method of estimation penetration depth*, Phys. Rev. B **61**, 6366 (2000).
- [52] C.P. Bean, *Magnetization of hard superconductors*, Phys. Rev. Lett. **8**, 250 (1962).
- [53] W.A. Fietz and W.W. Webb, *Hysteresis in superconducting alloys – temperature and field dependence of dislocation pinning in niobium alloys*, Phys. Rev. **178**, 657 (1969).
- [54] R.D. Boss, J.S. Briggs, E.W. Jacobs, T.E. Jones, and P.A. Mosier-Boss, *Preparation of superconducting K₃C₆₀ and Rb₃C₆₀ by precipitation from liquid ammonia*, Physica C **243**, 29 (1995).
- [55] M.W. Lee, M.F. Tai, S.C. Luo, and J.B. Shi, *Critical current densities in K₃C₆₀/Rb₃C₆₀ powders determined from AC/DC susceptibility measurements*, Physica C **245**, 6 (1995).
- [56] V. Buntar, *Investigation of inter- and intragrain currents in K₃C₆₀ single crystals*, Physica C **309**, 98 (1998).
- [57] V.A. Buntar and A.G. Buntar, *Critical current density and granularity in crystals of K₃C₆₀ fulleride*, Low Temp. Phys. **25**, 161 (1999).
- [58] E.F. Talantsev and J.L. Tallon, *Universal self-field critical current for thin-film superconductors*, Nat. Commun. **6**, 7820 (2015).
- [59] G. Els, P. Lemmens, G. Güntherodt, H.P. Lang, V. Thommen-Geiser, and H.-J. Güntherodt, *Determination of the superconducting energy gap of Rb₃C₆₀ by Raman scattering*, Physica C **235-240**, 2475 (1994).
- [60] Z. Zhang, C.-C. Chen, and C.M. Lieber, *Tunneling spectroscopy of M₃C₆₀ superconductors: the energy gap, strong coupling, and superconductivity*, Science **254**, 1619 (1991).
- [61] M.Q. Ren, S. Han, S.Z. Wang, J.Q. Fan, C.L. Song, X.C. Ma, and Q.K. Xue, *Direct observation of full-gap superconductivity and pseudogap in two-dimensional fullerenes*, Phys. Rev. Lett. **124**, 187001 (2020).
- [62] S. Sasaki, A. Matsuda, and C.W. Chu, *Fermi-liquid behavior and BCS s-wave pairing of K₃C₆₀ observed by ¹³C-NMR*, J. Phys. Soc. Jpn. **63**, 1670 (1994).
- [63] L. Degiorgi, G. Briceno, M.S. Fuhrer, A. Zettl, and P. Wachter, *Optical measurements of the superconducting gap in single-crystal K₃C₆₀ and Rb₃C₆₀*, Nature **369**, 541 (1994).
- [64] A.M. Clogston, *Upper limit for the critical field in hard superconductors*, Phys. Rev. Lett. **9**, 266 (1962).
- [65] L.W. Gruenberg and L. Gunther, *Fulde-ferrell effect in type-II superconductors*, Phys. Rev. Lett. **16**, 996 (1966).
- [66] K. Prassides, J. Tomkinson, C. Christides, M.J. Rosseinsky, D.W. Murphy, and R.C. Haddon, *Vibrational spectroscopy of superconducting K₃C₆₀ by inelastic neutron scattering*, Nature **354**, 462 (1991).
- [67] C.M. Varma, J. Zaanen, and K. Raghavachari, *Superconductivity in the fullerenes*, Science **254**, 989 (1991).
- [68] F.C. Zhang, M. Ogata, and T.M. Rice, *Attractive interaction and superconductivity for K₃C₆₀*, Phys. Rev. Lett. **67**, 3452 (1991).
- [69] M. Schluter, M. Lannoo, M. Needels, G.A. Baraff, and D. Tománek, *Electron-phonon coupling and superconductivity in alkali-intercalated C₆₀ solid*, Phys. Rev. Lett. **68**, 526 (1993).
- [70] G.H. Chen and W.A. Goddard III, *Mechanism of superconductivity in K₃C₆₀*, Proc. Natl. Acad. Sci. U.S.A. **90**, 1350 (1993).
- [71] J.E. Han, O. Gunnarsson, and V.H. Crespi, *Strong superconductivity with local Jahn-Teller phonons in C₆₀ solids*, Phys. Rev. Lett. **90**, 167006 (2003).
- [72] Y. Nomura, S. Sakai, M. Capone, and R. Arita, *Unified understanding of superconductivity and Mott transition in alkali-doped fullerenes from first principles*, Sci. Adv. **1**, e1500568 (2015).
- [73] O.V. Dolgov and I.I. Mazin, *Ginzburg-Landau analysis of superconducting K₃C₆₀*, Solid State Commun. **81**, 935 (1992).
- [74] S.C. Erwin and W.E. Pickett, *Theoretical Fermi-surface properties and superconducting parameters for K₃C₆₀*, Science **254**, 842 (1991).
- [75] L. Lu, V.H. Crespi, M.S. Fuhrer, A. Zettl, and M.L. Cohen, *Universal form of Hall coefficient in K and Rb doped single crystal C₆₀*, Phys. Rev. Lett. **74**, 1637 (1995).
- [76] P.A. Heiney, J.E. Fischer, A.R. McGhie, W.J. Romanow, A.M. Denenstien, J.P. McCauley Jr., A.B. Smith, and D.E. Cox, *Orientational ordering transition in solid C₆₀*, Phys. Rev. Lett. **66**, 2911 (1991).
- [77] S.E. Barrett and R. Tycko, *Molecular orientational dynamics in K₃C₆₀ probed by two-dimensional nuclear magnetic resonance*, Phys. Rev. Lett. **69**, 3754 (1992).
- [78] V. Buntar, F.M. Sauerzopf, and H.W. Weber, *Lower critical fields of alkali-metal-doped fullerene superconductors*, Phys. Rev. B **54**, 9651(R) (1996).
- [79] C.C. Chen and C.M. Lieber, *Synthesis of pure ¹³C₆₀ and determination of the isotope effect for fullerene superconductors*, J. Am. Chem. Soc. **114**, 3141 (1992).
- [80] A.A. Zakhidov, K. Imaeda, D.M. Petty, K. Yakushi, H. Inokuchi, K. Kikuchi, I. Ikemoto, S. Suzuki, and Y. Achiba, *Enhanced isotope effect in ¹³C-rich superconducting M_xC₆₀ (M=K, Rb): Support for vibronic pairing*, Phys. Lett. A **164**, 355 (1992).
- [81] P. Auban-Senzier, G. Quirion, D. Jerome, P. Bernier,

- S. Della-Negra, C. Fabre, and A. Rassat, *Isotope effect on 82% ^{13}C substituted K_3C_{60}* , *Synthetic Met.* **56**, 3027 (1993).
- [82] M. Riccò, F. Gianferrari, D. Pontiroli, M. Belli, C. Bucci, and T. Shiroka, *Unconventional isotope effects in superconducting fullerenes*, *Europhys. Lett.* **81**, 57002 (2008).
- [83] S. Chakravarty, S.A. Kivelson, M.I. Salkola, and S. Tewari, *Isotope effect in superconducting fullerenes*, *Science* **256**, 1306 (1992).
- [84] N.W. Ashcroft and M. Cyrot, *Isotope effect in metallofullerenes*, *Europhys. Lett.* **23**, 605 (1993).
- [85] Y.J. Uemura, L.P. Le, G.M. Luke, B.J. Sternlieb, W.D. Wu, J.H. Brewer, T.M. Riseman, C.L. Seaman, M.B. Maple, M. Ishikawa *et al.*, *Basic similarities among cuprate, bismuthate, organic, cheverl-phase, and heavy-Fermion superconductors shown by penetration-depth measurements*, *Phys. Rev. Lett.* **66**, 2665 (1991).
- [86] Y.J. Uemura, *Dynamic superconductivity responses in photoexcited optical conductivity and Nernst effect*, *Phys. Rev. Mater.* **3**, 104801 (2019).
- [87] C.H.P. Wen, H.C. Xu, Q. Yao, R. Peng, X.H. Niu, Q.Y. Chen, Z.T. Liu, D.W. Shen, Q. Song, X. Lou *et al.*, *Unveiling the superconducting mechanism of $\text{Ba}_{0.51}\text{K}_{0.49}\text{BiO}_3$* , *Phys. Rev. Lett.* **121**, 117002 (2018).
- [88] V. Petricek, M. Dusek, and L. Palatinus, *Crystallographic computing system JANA2006: General features*, *Z. Kristallogr.* **229**, 345 (2014).
- [89] A. Le Bail, *Whole powder pattern decomposition methods and applications: A retrospection*, *Powder Diffr.* **20**, 316 (2005).
- [90] L.J. Van der Pauw, *A method of measuring specific resistivity and Hall effect of discs of arbitrary shape*, *Philips Res. Rep.* **13**, 1 (1958).